Polymer Testing 102 (2021) 107310

Contents lists available at ScienceDirect

Polymer Testing

journal homepage: www.elsevier.com/locate/polytest

Experimental investigation for modeling the hardening of thermosetting polymers during curing

Bilen Emek Abali [a,*], Mert Yücel Yardımcı [c,d], Michele Zecchini [b], Gilda Daissè [b], Flávio H. Marchesini [e], Geert De Schutter [c], Roman Wan-Wendner [b,c]

[a] Uppsala University, Division of Applied Mechanics, Department of Materials Science and Engineering, Box 534, 751 21 Uppsala, Sweden
[b] University of Natural Resources and Life Sciences, Vienna, Christian Doppler Laboratory LiCRoFast, Peter-Jordan-Straße 82, 1190 Vienna, Austria
[c] Ghent University, Department of Structural Engineering and Building Materials, Magnel–Vandepitte Laboratory, Technologiepark-Zwijnaarde 60, Zwijnaarde 9052 Ghent, Belgium
[d] Istanbul Okan University, Department of Civil Engineering, Tuzla, 34959, Istanbul, Turkey
[e] Ghent University, Department of Materials, Textiles and Chemical Engineering, Technologiepark-Zwijnaarde 130, Zwijnaarde 9052 Ghent, Belgium

ARTICLE INFO

Keywords:
Thermosetting polymers
Curing
Rheometer
Inverse analysis

ABSTRACT

During curing of thermosetting polymers, crosslinking results in hardening or stiffening of the material. In electronics, for example in encapsulating integrated circuits (die bonding), thermosets are fully cured in a controlled environment (under UV-light or within a thermal oven) such that the highest stiffness possible has been achieved. In building materials, specifically in thermosets used in fastening systems (adhesive anchoring), hardening occurs at environmental temperature. Daily temperature variations alter the curing process and possibly lead to a lower stiffness. We demonstrate a modeling approach for the mechanical response dependency on the degree of cure by means of rheometer measurements under a specific temperature profile. Precisely, we perform oscillatory rheometric tests and convert the storage and loss moduli to material parameters depending on the degree of cure. Moreover, the temperature dependency as well as chemical shrinkage have been determined by the same experimental protocol. The presented approach has been applied to a commercially available (epoxy) thermoset used as an adhesive. We have observed a hardening after a gelation point of 0.7 and an adequate fit for mechanical response by polynomial functions of degree four.

1. Introduction

Description of a rheological behavior in polymer systems is challenging because of its intrinsic non-linear nature [1–4]. One class of polymers, called thermosetting polymers, starts an irreversible curing process under an activation energy supplied from the environment. This energy is in form of UV-light or temperature. Especially for two components—one is the base material and the other is the hardener—the chemical reaction starts after mixing the components, where individual chains form covalent bonds by using subgroups leading to crosslinking. This process is exothermal and often autocatalytic, so once the reaction starts, it continues effected by the energy produced by its own exothermal reaction. Generally speaking, the curing process increases the stiffness of the material, thus, the mixture as a fluid material starts behaving as a solid body. The transition from fluid to solid is called the gelation point. We aim at studying the stiffening process from the fluid to the solid behavior.

Curing is modeled by a scalar quantity called degree of cure, which is normalized to the maximum possible curing state. Mechanical response depends on this degree of cure. One particular application in structural engineering relies on the epoxy based adhesives used in fastening systems. A post-installed rod is anchored to the hardened concrete by drilling a hole and attaching with the adhesive [5–7]. The curing process starts immediately after filling the hole by the two component mixture and it continues at the ambient temperature. Cure kinetics and mechanical response depending on the degree of cure is of interest in thermosetting polymers also in processing such as additive manufacturing [8,9]. We stress that the curing process is irreversible and the degree of cure varies between 0 and 1. The cure kinetics is well studied for different systems with differential scanning calorimetry (DSC), for example we refer to [10,11] for phenomenological modeling and [12–14] for formal analysis. In this work, we highlight the relation of the mechanical response with the degree of cure. Mechanical dynamical experiments exist in the literature [15–17], they often report

* Corresponding author.
E-mail address: bilenemek@abali.org (B.E. Abali).

https://doi.org/10.1016/j.polymertesting.2021.107310
Received 6 March 2021; Received in revised form 22 July 2021; Accepted 1 August 2021
Available online 28 August 2021

the results without obtaining a material equation. We briefly explain the model used in this work and simulate the experimental process in order to obtain the degree of cure during experimental characterization. The main purpose is a methodology for combining mechanical response dependence on the degree of cure.

A rotational viscometer (rheometer) deforms the specimen in torsion, which is simple shear, monotonously or under a cyclic motion. The cyclic or so-called oscillatory measurement is harmonic that is optimized for linear rheology with outputs of so-called storage and loss moduli, responsible for reversible (elastic) and irreversible (dissipative, viscous) processes, respectively. Rheological analyses are well-established for a variety of materials, from cellulose [18] to cement paste [19–21]. Extension to nonlinear models is possible as well, we refer to [22,23] in the case of a rheometer, [24,25] for postprocessing, [26,27] for modeling approaches.

In order to use the experimental results in simulations, we need an adequate material model [28]. Therefore, we propose a methodology by presenting experimental results and explain a possible connection by introducing a scalar function for the dependency between mechanical response and the degree of cure. We model the experimentally observed behavior accurately by determining all parameters by means of a nonlinear regression. This simple yet effective methodology can be used for all chemically hardening substances like thermosets. We demonstrate the approach by applying it to a commercially available epoxy based thermosetting polymer used as an adhesive in anchors.

2. Mechanical response

In linear rheology, the stress-strain relation is modeled by using simple rheological models composed of springs and dashpots in series and parallel. In the case of rheometric experiments, shear stress and shear strain are modeled by this mechanical model. Especially for solid bodies showing a creep behavior, which is the case for the examined thermosetting polymer, the standard linear solid model, also called Zener model, is used between the shear stress component, σ, and shear strain component, ε, as follows:

$$\sigma + K_1\dot{\sigma} = K_2\varepsilon + K_3\dot{\varepsilon} \,, \tag{1}$$

under the assumption that the same relation holds for all components of stress and strain (co-linearity). The coefficients for a spring under shear, G_1, and dashpot, η_1, in parallel connected to a spring, G_0, in series read

$$K_1 = \frac{\eta_1}{G_0+G_1} \,, \quad K_2 = \frac{G_0G_1}{G_0+G_1} \,, \quad K_3 = \frac{G_0\eta_1}{G_0+G_1} \,. \tag{2}$$

To be determined material constants are linear springs denoting moduli, G_i, and a linear dashpot with the viscosity, η_1. Under the constant mechanical loading with constant (in time) stress, σ_0, the solution of this ordinary differential equation in time reads

$$\varepsilon(t) = J(t)\sigma_0 \,, \quad J(t) = \frac{1}{G_0} + \frac{1}{G_1}\left(1 - \exp\left(-\frac{G_1}{\eta_1}t\right)\right) \,. \tag{3}$$

The creep response, $J(t)$, is to be determined by experiments (not studied herein). The modulus, G_1, in Pa and viscosity, η_1 in Pa s are also converted to a creep time, $\tau_1 = \eta_1/G_1$, which indicates the response time of the viscous relation. Depending on the underlying material, for example different chain lengths of the thermosets, we expect that different response times affect the system response. In this case, the generalized Zener model reads

$$J(t) = \frac{1}{G_0} + \sum_i \frac{1}{G_i}\left(1 - \exp\left(-\frac{t}{\tau_i}\right)\right) \,, \quad \tau_i = \frac{\eta_i}{G_i} \,. \tag{4}$$

All moduli terms, G_i, incorporate a reversible (elastic) response and η_i (correspondingly τ_i) an irreversible (dissipative, viscous) response. The only assumption is that the material behaves linearly, for a nonlinear response and its modeling, we refer to [29, Sect. 9] for a detailed investigation regarding oscillatory measurements.

3. Experiments in rheometer and calorimeter

All measurements were performed at the Magnel–Vandepitte Lab at Ghent University (Belgium) on an Anton Paar Modular Compact Rheometer MCR 102 and its software running on a Windows 10 computer. Disposable aluminum upper plates were used on a flat bottom surface that is covered by an aluminum tape. A photo depicting the configuration is seen in Fig. 1. The bottom plate was fixed and the upper plate was driven by a given sinusoidal function steering the motion. All measurements were displacement controlled in order to make sure that the deformation was within the small displacement regime, thus, elastic. At a constant frequency of 1 Hz and 0.1% amplitude, shear strain was given by an internal feedback controller regulating the torque for the torsional motion leading to simple shear. By using D-PP25 upper plate complied with the ISO6721-10, we measured the storage and loss moduli by using the conversion factors, which utilize a mean shear rate and stress as described in DIN 53018. The diameter of the upper plates was 25.000 mm regarding the datasheet, i.e. with 0.1 µm dimensional accuracy, and the specimens were trimmed in all experiments by the same person in order to increase the repeatability. The initial height was set to 1 mm as also suggested in standards. The volume of the specimen was depending on the height, which did change during crosslinking known as the chemical shrinkage. Normal force and current thickness were recorded as well. Precise active temperature steering was acquired with installed Peltier plates (air ventilation). At the bottom plate the temperature was measured and assumed to be constant through the 1 mm thickness. Prior to starting each rheological test, the temperature of the bottom plate was reduced to 10 °C and then the material to be tested was put on the bottom plate. After arranging the 1 mm material thickness (corresponding to the gap distance between the parallel plates) the rheological protocol was initiated. During the rheological test:

- step I, temperature increase from 10 °C to 85 °C in 10 min;
- step II, constant temperature at 85 °C for 50 min;
- and step III, temperature decrease back to 10 °C in 10 min.

The outcome of the measurement, which is used in the inverse analysis, is visualized in Fig. 2. The protocol was selected for the following reason. First, in step I, a sufficiently quick temperature increase was realized in order to reach 85 °C being slightly higher than the glass transition temperature at the fully cured state. This choice ensured the complete curing without vitrification. Moreover, the increase was quick enough that the gelation point was not reached during this heating phase. We stress that the 1 mm thickness of the specimen is key for enabling this relatively fast heating process. Second, in step II, there was a constant (in time) temperature state designed for isothermal curing. We emphasize that the chemical reaction had been exothermal such that the active temperature control was of importance. The active temperature control is a standard functionality in all Peltier augmented bottom plate rheometers. The step II was 50 min long, which was indeed adequate for the specific choice of the specimen material. Third, step III was a cooling down process for measuring the temperature dependency to be analyzed in the next section.

We observed that the suggested temperature variation was reasonable with the air ventilation Peltier plates. Only at the change from the linear increase to the steady state, a slight deviation was recorded right after 10 min corrected by the feedback controller to the set value. The disposable upper plate was necessary since the adhesive attained a high stiffness making it otherwise challenging to peal off the adhering surface. Thus, the upper plate itself was often deformed by getting off the specimen. For each experiment, a new upper plate was used. As the material, a commercial product was used—epoxy based adhesive thermosetting polymer for fastening applications. This product comes in a cartridge with a static mixer ensuring the same mixing ratio of the base and hardener. For each specimen, a new cartridge was used. The time between mixing at room temperature until the start of the

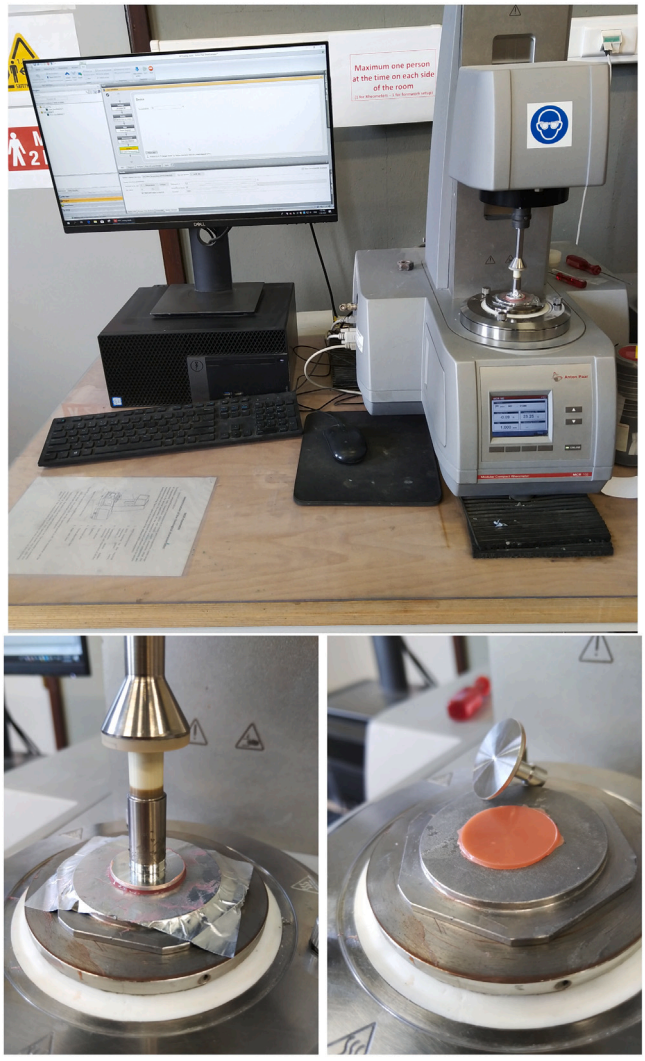

Fig. 1. Experimental setup, top: equipment, bottom left: parallel plate-plate with 1 mm thick specimen, bottom right: after the experiment, hardened specimen of 25 mm diameter taken out of the upper plate, put behind the specimen.

experiment was less than a minute, so we presumed that the curing is insignificant in this short period (regarding the time until the gelation point). In order to minimize the air trapping within the specimen, the mixture was put into the middle of the bottom plate and squeezed by the upper plate to the set 1 mm thickness. No preforming was used.

Differential Scanning Calorimetry (DSC) measurements were executed in Tulln (Austria) for measuring the heat produced during the curing reaction. Specifically, a Netzsch DSC F3 Maia (Netzsch Geraetebau GmbH, Germany) was utilized for all experiments with its software. The temperature was controlled, so that isothermal measurements for different temperature values of 30, 40, 60, and 80 °C were applied. In each experiment, the heat flux was recorded that was necessary to hold the temperature constant during the autocatalytic chemical process. Around 10 mg of the mixed, fresh material was used in a cell that contained both the sample and a reference. Mass of specimen was measured prior to measurement and assumed to remain constant—we ignored possible gases leaving the specimen during the chemical process. The highest temperature of 80 °C was adequate for obtaining a fully cured state. This statement was examined by an additional dynamic test from 20 °C to 100 °C. In this way, we observed by the recorded heat flux that the isothermal experiment at 80 °C did result in a complete curing. The enthalpy was calculated based on this experiment with the complete curing. By using the enthalpy of the fully cured measurement, we normalized all experiments as shown in Fig. 3. By using additional experiments, the glass transition temperature for different degrees of cure was obtained and used for modeling the curing phenomenon in the following section. Effected by the glass transition temperature dependency on the degree of cure, lower temperature isothermal experiments failed to achieve a fully cured state, known as vitrification.

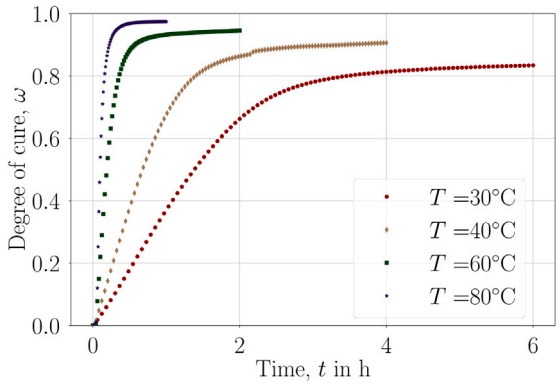

Fig. 3. DSC isothermal measurement results at 30, 40, 60, and 80 °C after normalizing, time, t, in hour as x-axis and degree of cure, ω, as y-axis.

4. Analysis of results

In order to examine the repeatability of the procedure, we demonstrate three subsequent experiments where the storage and loss moduli are obtained directly as results shown in Fig. 4(a) and (b). Obviously, at first sight, the repeatability was missing. Especially the final stiffness values represented by the storage values after 60 min were different. Approximately after 17 minutes, we observed the so-called gelation point, ω_g, where the curing surpasses to a solid state with an increased

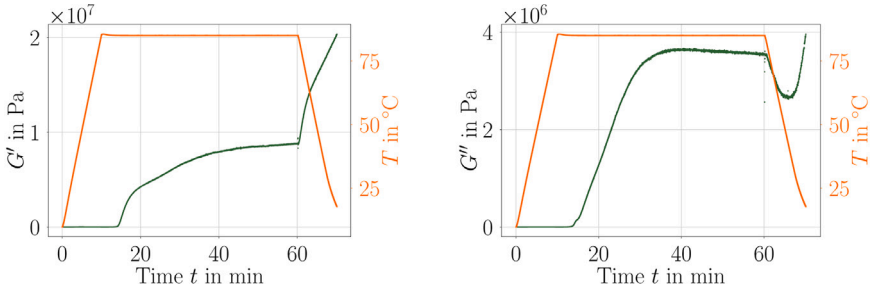

Fig. 2. Measurables G' (left) and G'' (right) are shown over time in min. On the right axes, the controlled temperature is plotted indicating from 10 °C to 85 °C in 10 min, holding for 50 min, cooling down to 20 °C in 10 min.

crosslinking density rate such that the hardening process was accelerated. As this gelation point was visible around the same time for all repetitions, we examined the hardening behavior by normalizing the values by their end values. As seen in Fig. 4(c) and (d), the normalized results show an adequate consistency. Thus, we conclude that the hardening procedure is the same; however, the overall stiffness differs.

Under taking off the specimen by bending and peeling off without damage, we compared their porosity values because of trapped air (bubbles) in Fig. 5 by a visual inspection. Although the preparation was done by the same person, the porosity was different and one of three specimens was "bubble-free." The air trapping into the specimen is expected in real life conditions as well and we report that the stiffness is depending on this significantly, at least for thin structures as herein. A volumetric ratio like porosity seems to be inadequate for this cylindrical geometry, where the stress distribution fails to be constant along the radial direction. We circumvent ourselves from a relation between porosity and stiffness in general owing to the lack of the statistical relevance. We emphasize that each test is more than one hour using disposable upper plate and a new cartridge.

The storage modulus, G', is responsible for the reversible deformation. Analogously, the loss modulus, G'', is steered by the irreversible response. By normalizing the storage modulus by G'_{m} and loss modulus by G''_{m}, it is obvious that the underlying experiment may be used to establish the hardening relation with respect to the degree of cure. Therefore, we propose to decompose the mechanical parameters, E_i and η_i that depend on the temperature, T, and degree of cure, ω, in a multiplicative way

$$E_i(T,\omega) = \bar{E}_i \theta_E(T)\phi_E(\omega) \ , \quad \eta_i(T,\omega) = \bar{\eta}_i \theta_\eta(T)\phi_\eta(\omega) \ , \tag{5}$$

with the amplitudes, $\bar{E}_i$, $\bar{\eta}_i$, to be determined by additional (creep) tests. The proposed decomposition has the formal benefit of combining different measurements:

- one mechanical (creep) test for determining the amplitudes, $\bar{E}_i$, $\bar{\eta}_i$, at the reference temperature, $\theta_E = \theta_\eta = 1$, and the fully cured state, $\phi_E = \phi_\eta = 1$ (not demonstrated herein),
- the presented rheometer test during the curing process in order to acquire, ϕ_E, ϕ_η, at an isothermal state
- and another thermal test for detecting the temperature dependency by fitting $\theta_E(T)$, $\theta_\eta(T)$ at the fully cured state, $\phi_E = \phi_\eta = 1$.

As we need a normalized ϕ_E, ϕ_η in order to obtain $\phi_E(\omega = 1) = \phi_\eta(\omega = 1) = 1$, it is obvious for the linear viscoelastic material response to propose

$$\phi_E = \frac{G'}{G'_{\mathrm{m}}} \ , \quad \phi_\eta = \frac{G''}{G''_{\mathrm{m}}} \ . \tag{6}$$

By using the proposed multiplicative decomposition leading to a separation of concerns, the amount of experiments are reduced drastically. The sole assumption for this decomposition relies on the same dependency for all curing states. From a physical chemistry point of view, this assumption is often taken for granted. As we are interested above the gelation point, ω_{g}, it is admissible to claim that the crosslinking above the gelation point hardens the material without significantly affecting its material response. In other words, a viscoelastic response above the gelation point fails to switch to a brittle material response or *vice versa*.

We aim for determining the hardening relations, $\phi_E(\omega)$, $\phi_\eta(\omega)$, uniquely. In this regard the temperature rate is assumed to be insignificant. This claim was examined by additional experiments as seen in Fig. 6. For different temperature rates, the response was qualitatively the same. After converting the results by means of the degree of cure, in the forthcoming section, we will observe that the results were quantitatively the same as well.

5. Modeling the curing process

An exothermal chemical process is of autocatalytic character for the curing of thermosets [30–33]; therefore, once the process starts, it evolves until the fully cured state has been reached. However, the reaction speed may be so slow that the process is practically observed as stopped—vitrification. As the energy threshold for this phenomenon, a so-called glass transition temperature, T_{g}, is introduced. The glassy regime has its name because viscous fluid (here resin) shows a power law increase in viscous characteristics [34] as temperature decreases below the glass transition temperature. Thus, below and above T_{g}, the differing curing rates are taken into account, we refer to phenomenological observations [35] and models based on the free volume reduction [36]. We characterize glassy and rubbery states as occurring simultaneously with their individual autocatalytic reactions involving a diffusion controlled mechanism, K_{diff}, as well as a chemically steered mechanism, K_{chem}. This model has been introduced in [37] and amended in [38]. Effected by the epoxy based mixture used herein, we model primary and secondary amines via autocatalysis and impurity catalysis (denoted by c in index) by the following evolution equation:

$$\begin{gathered}\dot{\omega} = K_1(1-\omega)^2\left(\omega + \frac{K_{1c}}{K_1}\right) \ , \quad \frac{1}{K_1} = \frac{1}{K_{1,\mathrm{chem}}} + \frac{1}{K_{\mathrm{diff}}} \ , \quad \frac{1}{K_{1c}} = \frac{1}{K_{1c,\mathrm{chem}}} + \frac{1}{K_{\mathrm{diff}}} \ , \\ K_{1,\mathrm{chem}} = A_3 \exp\left(-\frac{E_3}{RT}\right) \ , \quad K_{1c,\mathrm{chem}} = A_4 \exp\left(-\frac{E_4}{RT}\right) \ , \\ K_{\mathrm{diff}} = k_{T_{\mathrm{g}}} \exp\left(\frac{C_1(T-T_{\mathrm{g}})}{C_2 + |T-T_{\mathrm{g}}|}\right) \ .\end{gathered} \tag{7}$$

Modeled by the Williams–Landel–Ferry (WLF) equation in the rubbery regime, the diffusion rate, K_{diff}, is several orders of magnitude greater than the chemical rate, K_{chem}. As aforementioned, in the glassy state, diffusion rate is nearly zero compared to the chemical rate. Therefore, although the curing process is evolving, we measure no change in the degree of curing known as vitrification. Under these conditions, instead of hours, the reaction needs years to be completed. Modeling T_{g} needs to be established by additional calorimetric measurements by applying a fit function [38–41], as follows:

$$T_{\mathrm{g}} = \exp\left(\frac{(1-\omega)\ln(T_{\mathrm{g},0}) + \Delta C \omega \ln(T_{\mathrm{g},\infty})}{(1-\omega) + \Delta C \omega}\right) \ . \tag{8}$$

For determining all the parameters $T_{\mathrm{g},0}$, $T_{\mathrm{g},\infty}$, ΔC as well as C_1, C_2, $k_{T_{\mathrm{g}}}$, A_3, A_4, E_3, E_4 from calorimetry experiments, there exists different proposals in the literature [42,43] based on simplifications that parameters may be obtained separately. Instead of following these protocols, we solve the inverse analysis directly by a method developed in Python language. In this way, the proposed method is also applicable for different evolution equations than given by Eq. (7). Technically speaking, the degree of cure is used for computational models [44–47] in a coupled manner. However, in the experimental setting, as the temperature distribution is held constant within the specimen, we decouple the problem and reduce it to an ordinary differential equation. This equation for the evolution of degree of cure is solved numerically by SciPy packages in Python, specifically, the fourth-order Runge–Kutta is used with a tolerance value of 10^{-6} in each iteration. By using an optimization problem based on minimization of squared error by means of trust region reflective algorithm augmented by a Cauchy loss, we acquire parameters as compiled in Table 1 and the agreement with the experimental results are depicted in Fig. 7. For details of the exact procedure and DSC curves, we refer to [48].

We obtain the degree of cure, ω, over time as visualized in Fig. 8. By using the degree of cure simulation for different protocols with two distinct temperature rates, all experimental results are compared by using Eq. (6). This comparison is of interest in terms of repeatability and to be depicted in Fig. 9. Around $\omega_{\mathrm{g}} = 0.7$ we observe the gelation point and around $\omega = 0.85$ we observe that half of the stiffness has been reached. Different cartridges and tests under different temperature

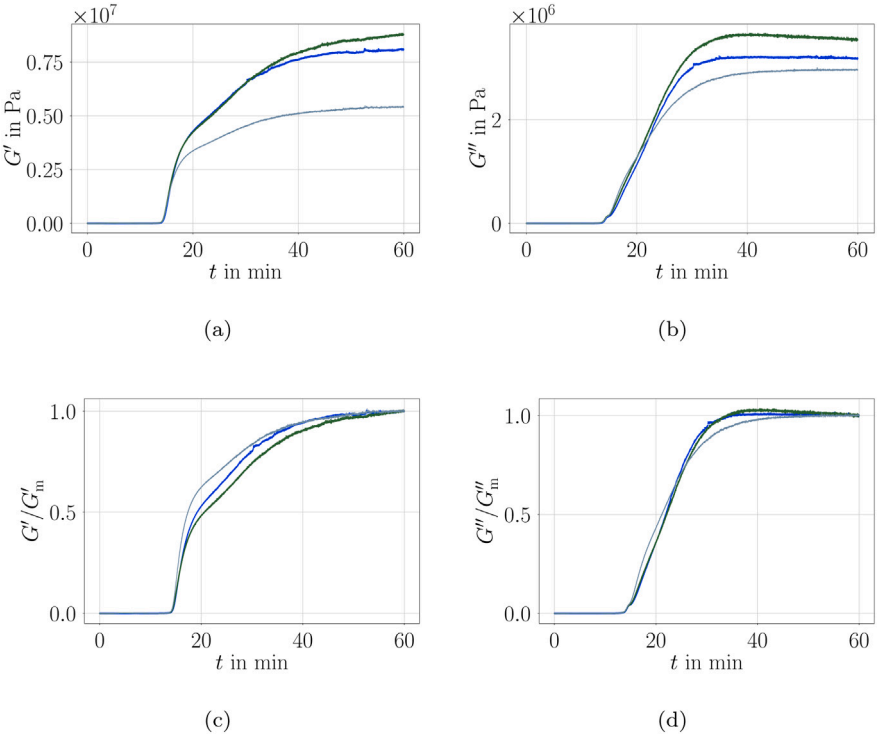

Fig. 4. Three subsequent measurements by the same protocol with storage modulus, G' in pascal, (a) and loss modulus, G'' in pascal, (b) over time, t in minute, during hardening. By maximum moduli, G'_{m}, G''_{m}, normalized results, (c) and (d), showing the consistency of the hardening over time and pointing out the deviation of the final stiffness but not the hardening procedure.

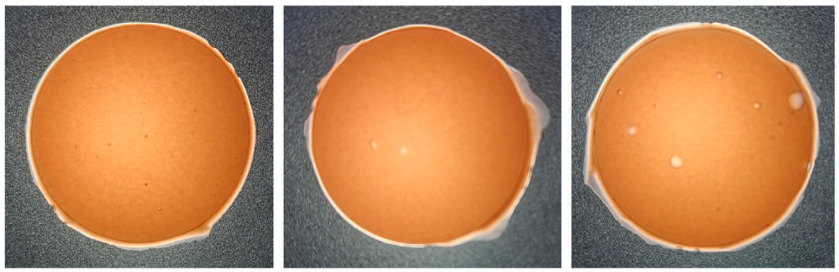

Fig. 5. Specimens of 1 mm thicknesses after the experiment, left: no visible bubbles, middle: two visible bubbles, right: three large and three small bubbles are visible.

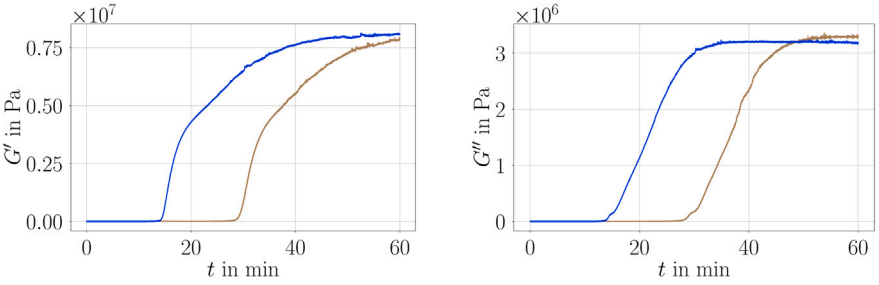

Fig. 6. Measurements with the aforementioned temperature rate (blue) and half of this value (brown) leading to the same value (both cases are "bubble-free"), time t in minute on x-axis and storage, loss moduli, G', G'' on y-axes.

rates are reporting an adequate repeatability that is demonstrating the feasibility of the assumptions used herein. Hence, we conclude that ϕ_E and ϕ_η functions are admissible in order to scale elastic and viscous parameters by means of the degree of cure. By using the cooling after reaching the fully cured state, as seen in Fig. 2, we obtain the temperature dependence, θ_E and θ_η, as shown in Fig. 10.

Furthermore, we obtain the volumetric shrinkage during curing, roughly after the gelation point, by measuring the current thickness of the specimen, t. Curing induced volumetric change is called chemical shrinkage. By using the protocol as above, we isolate the chemical shrinkage from the volumetric expansion due to the temperature change, since curing is obtained by a constant temperature. The gap between the upper and lower plates is initially 1 mm and is measured with 1 µm accuracy throughout the hardening. Hence, the strain is determined by measuring the thickness, t, leading to a shrinkage parameter for modeling the behavior depicted in Fig. 11.

Table 1
Determined material parameters for the curing model, for details, see material B in [48].

Variable	Value	Unit
$T_{g,0}$ =	9	°C
$T_{g,\infty}$ =	83	°C
ΔC =	0.332	–
A_3 =	96 748	1/s
A_4 =	11 012	1/s
E_3 =	46 440	G
E_4 =	49 462	G
k_{Tg} =	10.3	G
C_1 =	17.3	–
C_2 =	12.3	–

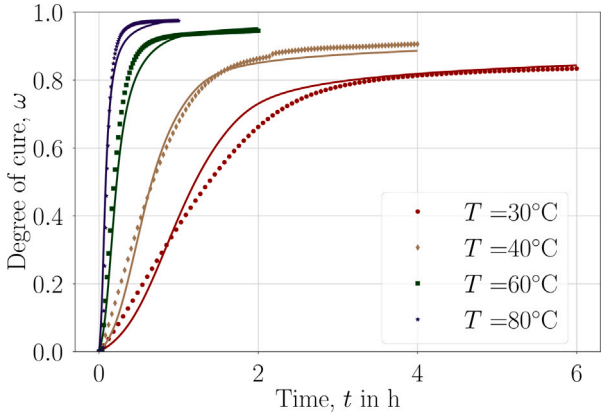

Fig. 7. Validation of inverse analysis results in modeling the curing phenomenon (continuous line) by means of the isothermal DSC experiments (dots), time, t in minute, on x-axis and degree of cure, ω, on y-axis..

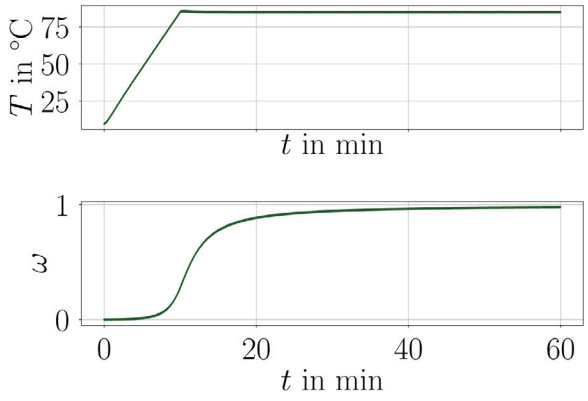

Fig. 8. Experimental temperature regulation (top) with temperature, T in degree Celsius, on y-axis given in time, t in minute, on x-axis. Expected curing evolution (bottom) given by degree of cure, ω, over time, t.

6. Inverse analysis for experiments

Using the experimental results G' and G'' as converted into ϕ_E and ϕ_η as shown in Fig. 9, there are five experimental data sets with each 3600 data points corresponding to one hour experiments with a 1 Hz data acquisition rate. All of the data has been used to fit a polynomial curve of degree four above the gelation point, ω_g, as follows:

$$\hat{\phi}_E(\omega) = \begin{cases} 0 & \text{, if } \omega < \omega_g \\ A_0 + A_1\omega + A_2\omega^2 + A_3\omega^3 + A_4\omega^4 & \text{, else} \end{cases} ,$$
$$\hat{\phi}_\eta(\omega) = \begin{cases} 0 & \text{, if } \omega < \omega_g \\ B_0 + B_1\omega + B_2\omega^2 + B_3\omega^3 + B_4\omega^4 & \text{, else} \end{cases} . \tag{9}$$

Table 2
Determined material parameters for cure and temperature dependencies in Eqs. (9), (11), (12).

$\phi_E(\omega)$	$\phi_\eta(\omega)$	$\theta_E(T)$	$\theta_\eta(T)$
$A_0 = -59.70$	$B_0 = 73.77$	$\bar{A}_0 = 646.00$	$\bar{B}_0 = 1265.98$
$A_1 = 123.16$	$B_1 = -179.69$	$\bar{A}_1 = -2647.25$	$\bar{B}_1 = -5313.72$
$A_2 = 2.99$	$B_2 = 24.62$	$\bar{A}_2 = 4054.93$	$\bar{B}_2 = 8363.15$
$A_3 = -136.03$	$B_3 = 200.35$	$\bar{A}_3 = -2735.37$	$\bar{B}_3 = -5848.28$
$A_4 = 70.58$	$B_4 = -118.05$	$\bar{A}_4 = 682.76$	$\bar{B}_4 = 1533.86$
$\omega_g = 0.80$			
$\omega_{\text{ref}} = 0.64$		$\beta = -5.25 \times 10^{-2}$	

Unknowns, $\boldsymbol{u} = \{\omega_g, A_0, A_1, A_2, A_3, A_4, B_0, B_1, B_2, B_3, B_4\}$, are determined by an inverse analysis, again by using Scipy packages and implementing an error minimization algorithm based on [49, Sect. 4.4]. This least squared error, which is the norm of the difference between fit functions, $\hat{\phi}_\times$ and experimental results $\phi_\times$, is minimized

$$\boldsymbol{u} = \underset{\text{w.r.t. } \boldsymbol{u}}{\arg\min} \left(\|\phi_E - \hat{\phi}_E\|^2 + \|\phi_\eta - \hat{\phi}_\eta\|^2 \right) . \tag{10}$$

Since the chosen fit functions result in a nonlinear minimization problem with many solutions (local minima), we use the Levenberg–Marquardt approach with a stochastic initial guess within $[-10, 10]$ for $A_\times$, $B_\times$ and $[0, 1]$ for ω_g running several times. Additionally, we utilize a penalty term for fulfilling results between $[0, 1]$ as well as zero at ω_g and one at $\omega = 1$. Analogously, the thermal dependency is approximated by a polynomial fit as follows:

$$\hat{\theta}_E(T) = \bar{A}_0 + \bar{A}_1 T + \bar{A}_2 T^2 + \bar{A}_3 T^3 + \bar{A}_4 T^4 ,$$
$$\hat{\theta}_\eta(T) = \bar{B}_0 + \bar{B}_1 T + \bar{B}_2 T^2 + \bar{B}_3 T^3 + \bar{B}_4 T^4 . \tag{11}$$

Polynomial degree of four is often used in standards. For the chemical shrinkage, we use the simple linear relation for an isotropic material with the strain depending only on the degree of cure, as follows:

$$\boldsymbol{\varepsilon}^{\text{sh}} = (\omega - \omega_{\text{ref}})\beta \boldsymbol{I} , \tag{12}$$

with the Kronecker delta (identity), $\boldsymbol{I}$. By referring to Fig. 11, the linear relationship is justified. Obviously, the strain is small such that we relate the thickness, t, and the initial thickness, $t_0 = 1$ mm, for obtaining the linear strain measure

$$\frac{t - t_0}{t_0} = (\omega - \omega_{\text{ref}})\beta . \tag{13}$$

By using the aforementioned optimization algorithm for this regression problem, we obtain unknowns β and ω_{ref}.

7. Results

The proposed method uses the decomposition of hardening related terms and thermal dependency as in Eq. (5). The inverse analysis results in the coefficients as compiled in Table 2. The inverse analysis is used by means of the curing model such that Table 1 is compulsory for the accuracy of utilizing Eqs. (9), (11), (12). The good agreement with the experimental results are depicted in Figs. 12, 13 showing that the error minimization has been working well. Both results in Figs. 12 and 13 are obtained independently, we basically assume that ω_g and ω_{ref} may be different. Shrinkage during curing is dominated by the crosslinking phenomena that is accelerated beyond the gelation point. Therefore, we expect ω_g and ω_{ref} have similar values, as observed in Table 2.

The fit in Fig. 12 is adequate owing to the polynomial function of degree four. For the fit in degree of cure dependency, using such a high order polynomial is essential in order to obtain the asymptotic approach to unity, $\phi_\times \to 1$, as degree of cure converges to the fully cured state, $\omega \to 1$.

Rheometer measurements by using the proposed protocol have been fruitful for obtaining the stiffness dependence on temperature and degree of cure; as well as the chemical shrinkage. The thermal expansion

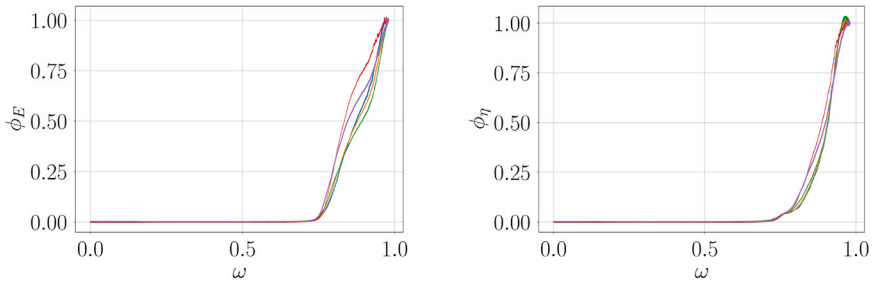

Fig. 9. Experimental mechanical properties to degree of cure relation, ϕ_E and ϕ_η, obtained from G' and G'' values in time, on y-axis versus degree of cure, ω, on x-axis.

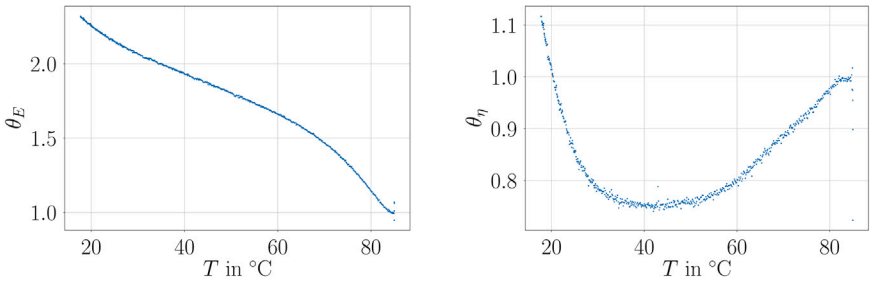

Fig. 10. Experimental θ_E and θ_η results, obtained from the cooling part in G' and G'' values in time, on y-axis versus degree of cure, ω, on x-axis.

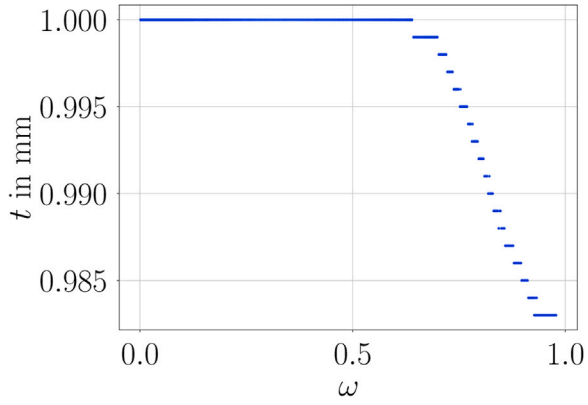

Fig. 11. Experimental thickness change, t in millimeter, on y-axis with respect to the degree of cure, ω, on x-axis. Thickness change is related to the chemical shrinkage effected by the curing, starting from a reference degree of cure around the gelation point until the fully cured state (measured under constant temperature).

is rather small such that for this material the accuracy of the current gap measurement is not sufficient, although the protocol allows this in step III by a temperature reduction after the fully cured state has been attained such that thermal expansion is isolated from the chemical shrinkage.

8. Conclusion

Thermosetting polymers harden and shrink during curing. We have investigated this phenomenon and modeled by using material equations with parameters acquired by an inverse analysis with the aid of open source packages from SciPy in the Python language. The presented approach may be adequate for several thermosetting polymers, herein, we have analyzed an epoxy based commercial product with superior mechanical properties used as an adhesive. As the mechanical properties depend on the degree of cure, we give a linear standard model known in rheology and investigate moduli and viscosities dependency on the degree of cure. Curing kinetics for such systems are well-known and we have used an evolution equation incorporating the glass transition temperature depending on the degree of cure. Parameters for this model are obtained by following standards with isothermal and dynamic calorimetry measurements. The work proposes a methodology based on a specifically chosen temperature profile during rheometer measurements. Degree of cure is simulated by the evolution equation and the methodology allows to obtain dependency of moduli and viscosities on the degree of cure. More specifically, we have used a temperature protocol with steps I, II, and III that leads to an isothermal curing process right before gelation point up to the fully cured state, which is then followed by a temperature decrease. This simple experimental setting allows obtaining enough information for setting up an inverse analysis and determine fit functions describing the complete dependency of moduli and viscosities on the degree of cure. Moreover, the final step allows to obtain the temperature dependency for an interval as well. Since the rheometer records the volume change, additionally, we have modeled the chemical shrinkage from the same set of experiments. The benefit of the proposed strategy is to use a standard rheometer with an active temperature control. No tweaks or special feedback controller tuning is necessary. The raw data is directly used in the inverse analysis. The same procedure may be used for other thermosets, especially in applications, where a complete curing is not expected, the mechanical response dependence on the degree of cure is of paramount importance.

Acknowledgment

This research was funded by the Christian Doppler Forschungsgesellschaft, Austria, Grant LICROFAST to Roman Wan-Wendner. The financial support by the Austrian Federal Ministry for Digital and Economic Affairs and the National Foundation for Research, Technology, and Development is acknowledged, as is the partial financial support by the Austrian Science Fund (FWF) under Grant P 31203-N32. The financial support by the Special Research Fund (BOF) of Ghent University,

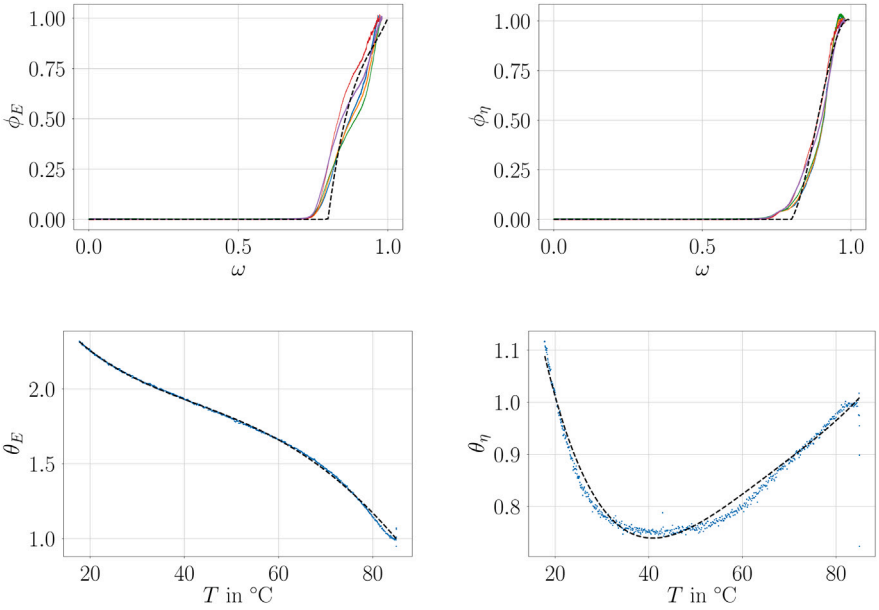

Fig. 12. Experimental ϕ_E and ϕ_η results as data points and the determined fit curves (dashed line) in Eqs. (9), (11).

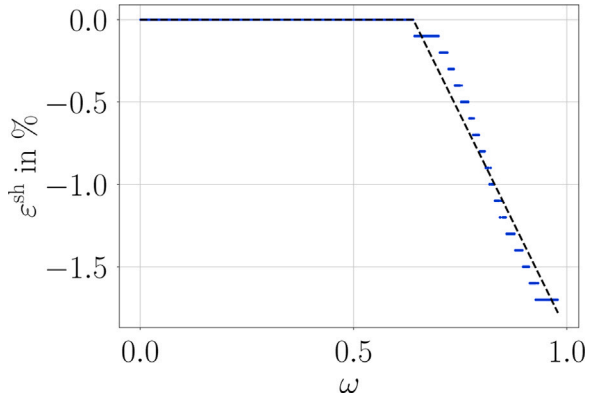

Fig. 13. Experimental results for the chemical shrinkage, ϵ^{sh} in percent, on y-axis versus degree of cure, ω, on x-axis, and determined fit curve (dashed line) by using the model in Eq. (12).

Belgium, Concerted Research Action (GOA), project BOF18-GOA-009, is acknowledged.

References

[1] G. Marrucci, G. Ianniruberto, et al., Modelling nonlinear polymer rheology is still challenging, Korea-Aust. Rheol. J. 17 (3) (2005) 111–116.

[2] R. Long, K. Mayumi, C. Creton, T. Narita, C.-Y. Hui, Rheology of a dual crosslink self-healing gel: Theory and measurement using parallel-plate torsional rheometry, J. Rheol. 59 (3) (2015) 643–665.

[3] B.E. Abali, C.-C. Wu, W.H. Müller, An energy-based method to determine material constants in nonlinear rheology with applications, Contin. Mech. Thermodyn. 28 (5) (2016) 1221–1246.

[4] I. Argatov, A. Iantchenko, V. Kocherbitov, How to define the storage and loss moduli for a rheologically nonlinear material? Contin. Mech. Thermodyn. 29 (2017) 1375–1387.

[5] G. Singer, G. Sinn, H.C. Lichtenegger, S. Veigel, M. Zecchini, R. Wan-Wendner, Evaluation of in-situ shrinkage and expansion properties of polymer composite materials for adhesive anchor systems by a novel approach based on digital image correlation, Polym. Test. 79 (2019) 106035.

[6] P.R. Bradler, J. Fischer, R. Wan-Wendner, R.W. Lang, Shear test equipment for testing various polymeric materials by using standardized multipurpose specimens with minor adaptions, Polym. Test. 75 (2019) 93–98.

[7] J. Fischer, P.R. Bradler, D. Schmidtbauer, R.W. Lang, R. Wan-Wendner, Long-term creep behavior of resin-based polymers in the construction industry, Mater. Today Commun. 18 (2019) 60–65.

[8] A. Redmann, P. Oehlmann, T. Scheffler, L. Kagermeier, T.A. Osswald, Thermal curing kinetics optimization of epoxy resin in digital light synthesis, Addit. Manuf. 32 (2020) 101018.

[9] A. Redmann, T.A. Osswald, A model for modulus development of dual-cure resin systems, Polym. Eng. Sci. 61 (3) (2021) 830–835.

[10] M. Kiasat, Curing Shrinkage and Residual Stresses in Viscoelastic Thermosetting Resins and Composites (Ph.D. thesis), Technical University of Delft, 2000.

[11] A. Lion, P. Höfer, On the phenomenological representation of curing phenomena in continuum mechanics, Arch. Mech. 59 (1) (2007) 59–89.

[12] R. Mahnken, Thermodynamic consistent modeling of polymer curing coupled to visco–elasticity at large strains, Int. J. Solids Struct. 50 (13) (2013) 2003–2021.

[13] M. Hossain, Modelling the curing process in particle-filled electro-active polymers with a dispersion anisotropy, Contin. Mech. Thermodyn. 32 (2020) 351–367.

[14] Z. Liao, M. Hossain, X. Yao, M. Mehnert, P. Steinmann, On thermo-viscoelastic experimental characterization and numerical modelling of VHB polymer, Int. J. Non-Linear Mech. 118 (2020) 103263.

[15] J.A. Kim, D.G. Seong, T.J. Kang, J.R. Youn, Effects of surface modification on rheological and mechanical properties of CNT/epoxy composites, Carbon 44 (10) (2006) 1898–1905.

[16] H. Rastin, M.R. Saeb, M. Nonahal, M. Shabanian, H. Vahabi, K. Formela, X. Gabrion, F. Seidi, P. Zarrintaj, M.G. Sari, Transparent nanocomposite coatings based on epoxy and layered double hydroxide: Nonisothermal cure kinetics and viscoelastic behavior assessments, Prog. Org. Coat. 113 (2017) 126–135.

[17] A. Zotti, S. Zuppolini, A. Borriello, M. Zarrelli, Thermal and mechanical characterization of an aeronautical graded epoxy resin loaded with hybrid nanoparticles, Nanomaterials 10 (7) (2020) 1388.

[18] B.E. Abali, Inverse analysis of cellulose by using the energy-based method and a rotational rheometer, Appl. Sci. 8 (8) (2018) 1354.

[19] Y. Qian, S. Ma, S. Kawashima, G. De Schutter, Rheological characterization of the viscoelastic solid-like properties of fresh cement pastes with nanoclay addition, Theor. Appl. Fract. Mech. 103 (2019) 102262.

[20] X. Dai, S. Aydın, M.Y. Yardımcı, K. Lesage, G. De Schutter, Effects of activator properties and GGBFS/FA ratio on the structural build-up and rheology of AAC, Cem. Concr. Res. 138 (2020) 106253.

[21] X. Dai, S. Aydin, M.Y. Yardımcı, K. Lesage, G. De Schutter, Influence of water to binder ratio on the rheology and structural build-up of alkali-activated slag/fly ash mixtures, Constr. Build. Mater. 264 (2020) 120253.

[22] R.H. Ewoldt, A. Hosoi, G.H. McKinley, New measures for characterizing nonlinear viscoelasticity in large amplitude oscillatory shear, J. Rheol. (1978-Present) 52 (6) (2008) 1427–1458.

[23] R. Ewoldt, P. Winter, J. Maxey, G. McKinley, Large amplitude oscillatory shear of pseudoplastic and elastoviscoplastic materials, Rheol. Acta 49 (2) (2010) 191–212.

[24] M. Wilhelm, Fourier-transform rheology, Macromol. Mater. Eng. 287 (2) (2002) 83–105.

[25] C. Klein, H. Spiess, A. Calin, C. Balan, M. Wilhelm, Separation of the nonlinear oscillatory response into a superposition of linear, strain hardening, strain softening, and wall slip response, Macromolecules 40 (12) (2007) 4250–4259.
[26] B.E. Abali, H. Yang, Magnetorheological elastomer's material modeling and parameter determination by using the energy-based method, in: B.E. Abali, H. Altenbach, F. dell'Isola, V.A. Eremeyev, A. Öchsner (Eds.), New Achievements in Continuum Mechanics and Thermodynamics, Springer Nature, Singapore, 2019, pp. 1–15.
[27] F.H. Marchesini, R.M. Oliveira, H. Althoff, P.R. de Souza Mendes, Irreversible time-dependent rheological behavior of cement slurries: Constitutive model and experiments, J. Rheol. 63 (2) (2019) 247–262.
[28] B.E. Abali, J. Vorel, R. Wan-Wendner, Thermo-mechano-chemical modeling and computation of thermosetting polymers used in post-installed fastening systems in concrete structures, Contin. Mech. Thermodyn. (2020) 1–20.
[29] B.E. Abali, Thermodynamically Compatible Modeling, Determination of Material Parameters, and Numerical Analysis of Nonlinear Rheological Materials (Ph.D. thesis), Technische Universität Berlin, Institute of Mechanics, 2014.
[30] L. Shechter, J. Wynstra, R.P. Kurkjy, Glycidyl ether reactions with amines, Ind. Eng. Chem. 48 (1) (1956) 94–97.
[31] M. Kamal, S. Sourour, Kinetics and thermal characterization of thermoset cure, Polym. Eng. Sci. 13 (1) (1973) 59–64.
[32] M.R. Kamal, Thermoset characterization for moldability analysis, Polym. Eng. Sci. 14 (3) (1974) 231–239.
[33] C. Heinrich, M. Aldridge, A.S. Wineman, J. Kieffer, A.M. Waas, K.W. Shahwan, Generation of heat and stress during the cure of polymers used in fiber composites, Internat. J. Engrg. Sci. (53) (2012) 85–111.
[34] C.A. Angell, Perspective on the glass transition, J. Phys. Chem. Solids 49 (8) (1988) 863–871.
[35] C.-S. Chern, G.W. Poehlein, A kinetic model for curing reactions of epoxides with amines, Polym. Eng. Sci. 27 (11) (1987) 788–795.
[36] H.-J. Flammersheim, J.R. Opfermann, Investigation of epoxide curing reactions by differential scanning calorimetry–formal kinetic evaluation, Macromol. Mater. Eng. 286 (3) (2001) 143–150.
[37] E. Rabinowitch, Collision, co-ordination, diffusion and reaction velocity in condensed systems, Trans. Faraday Soc. 33 (1937) 1225–1233.
[38] C.W. Wise, W.D. Cook, A.A. Goodwin, Chemico-diffusion kinetics of model epoxy-amine resins, Polymer 38 (13) (1997) 3251–3261.
[39] E. DiBenedetto, Continuity of weak solutions to a general porous medium equation, Indiana Univ. Math. J. 32 (1) (1983) 83–118.
[40] D. Hesekamp, H.C. Broecker, M.H. Pahl, Chemo-rheology of cross-linking polymers, Chem. Eng. Technol.: Ind. Chem.-Plant Equip.-Process Eng.-Biotechnol. 21 (2) (1998) 149–153.
[41] R. Venditti, J. Gillham, A relationship between the glass transition temperature (Tg) and fractional conversion for thermosetting systems, J. Appl. Polym. Sci. 64 (1) (1997) 3–14.
[42] M. Jouyandeh, S.M.R. Paran, A. Jannesari, D. Puglia, M.R. Saeb, Protocol for nonisothermal cure analysis of thermoset composites, Prog. Org. Coat. 131 (2019) 333–339.
[43] M. Nonahal, H. Rastin, M.R. Saeb, M.G. Sari, M.H. Moghadam, P. Zarrintaj, B. Ramezanzadeh, Epoxy/PAMAM dendrimer-modified graphene oxide nanocomposite coatings: Nonisothermal cure kinetics study, Prog. Org. Coat. 114 (2018) 233–243.
[44] M. Hossain, Modelling and Computation of Polymer Curing (Ph.D. thesis), Friedrich-Alexander-Universität Erlangen-Nürnberg, Germany, 2010.
[45] J. Mergheim, G. Possart, P. Steinmann, Modelling and computation of curing and damage of thermosets, Comput. Mater. Sci. 53 (1) (2012) 359–367.
[46] R.A. Sauer, A survey of computational models for adhesion, J. Adhes. 92 (2) (2016) 81–120.
[47] R. Landgraf, Modellierung und Simulation der Aushärtung polymerer Werkstoffe (Ph.D. thesis), TU Dresden, Germany, 2016.
[48] B.E. Abali, M. Zecchini, G. Daissè, I. Czabany, W. Gindl-Altmutter, R. Wan-Wendner, Cure kinetics and inverse analysis of epoxy-amine based adhesive used for fastening systems, Materials 14 (14) (2021) 3853.
[49] B.E. Abali, C. Cakiroglu, Numerische Merhoden Für Ingenieure, in: Lehrbuch, Technik : Technomathematik, Springer Vieweg, 2020.